ELSEVIER

Chemical Engineering Journal 113 (2005) 13–25

Chemical Engineering Journal

www.elsevier.com/locate/cej

SCR of NO with C_3H_6 in the presence of excess O_2 over Cu/Ag/CeO_2-ZrO_2 catalyst

N.A. Saidina Amin *, C.M. Chong

Chemical Engineering Department, Faculty of Chemical and Natural Resources Engineering, Universiti Teknologi Malaysia, 81310 Skudai, Johor, Malaysia

Received 9 December 2004; received in revised form 22 July 2005; accepted 2 August 2005

Abstract

The catalytic activity of a series of CeO_2-ZrO_2 mixed oxides in the selective catalytic reduction (SCR) of NO by C_3H_6 at 400 °C has been investigated. The NO reduction activity of pure CeO_2 is enhanced in the presence of Zr, reaching a maximum NO conversion with CeO_2(75)-ZrO_2(25) catalyst. Then, the catalytic performances of Cu(4)/Ag(1)/CeO_2 and Cu(4)/Ag(1)/CeO_2(75)-ZrO_2(25) catalysts were compared and the latter showed better activity especially in the low temperature region (250–350 °C). The stronger metal-support interaction and higher reducibility shown by the Cu(4)/Ag(1)/CeO_2(75)-ZrO_2(25) catalyst were believed to enhance its performance compared to Cu(4)/Ag(1)/CeO_2 catalyst by activating more C_3H_6 to selectively reduce NO within this temperature region. Central composite response surface design methodology was employed to study the effect of operating variables such as temperature, NO and C_3H_6 concentrations on the SCR of NO by C_3H_6 over Cu(4)/Ag(1)/CeO_2(75)-ZrO_2(25) catalyst and to determine the optimum value of operating variables for maximum NO conversion. Numerical results indicated that the optimum NO conversion of 82.89% is attained at reaction temperature = 415.38 °C, NO concentration = 1827.16 ppm and C_3H_6 concentration = 1908.13 ppm. The addition of water vapor to the reactant significantly decreased the NO conversion over Cu(4)/Ag(1)/CeO_2 and Cu(4)/Ag(1)/CeO_2(75)-ZrO_2(25), but the inhibition was more pronounced over Cu(4)/Ag(1)/CeO_2 catalyst.

Keywords: SCR; C_3H_6; Cu/Ag/CeO_2-ZrO_2; Central composite design; Water vapor

1. Introduction

Air pollution by nitrogen oxides (NO_x) is currently one of the most serious environmental problems. The conventional three-way catalyst shows low NO_x conversion in lean-burn exhaust that contains high concentration of O_2. NO_x storage-reduction (NSR) catalysts are a new class of prospective catalysts for the removal of nitrogen oxides from vehicle exhaust [1]. In lean-burn conditions, NO_x are stored at the surface of a Ba-containing catalyst under various forms (surface nitrites/nitrates). Later, the stored NO_x species will be reduced to N_2 over Pt or more generally, TWC-type catalyst when the engine operates in the stoichiometric or rich burn condition. The major drawback of the NSR catalyst is its sensitivity to SO_x due to the fact that surface sulphates are invariably more thermally stable compared to nitrate [2].

Alternatively, one of the most attractive techniques for NO_x removal is the selective catalytic reduction of NO_x in the exhaust gas by reducing agents. The most common catalytic procedure for selective catalytic reduction (SCR) is using ammonia or ammonia-containing compounds, mainly urea, as reducing agents. The process was discovered first by Cohn in 1961 [3]. It is the most effectively applied catalytic method of NO_x reduction in conventional electric power plants [4]. The disadvantages of this method include the need for a reducing agent to be temporarily stored on board the vehicle and for which there is yet no infrastructure for supply. High costs of the SCR-NH_3 installations are also a disadvantage. Furthermore, SCR-NH_3 systems may show ammonia slip, which can produce additional environmental pollution. Due

* Corresponding author. Tel.: +60 7 5535588; fax: +60 7 5581463.
E-mail address: noraishah@fkkksa.utm.my (N.A. Saidina Amin).

1385-8947/$ – see front matter © 2005 Elsevier B.V. All rights reserved.
doi:10.1016/j.cej.2005.08.001

to these reasons, the use of ammonia in vehicles is somewhat controversial [5,6].

The selective catalytic reduction of NO by hydrocarbons (SCR-HC) in the presence of excess O_2 currently attracts great attention as a promising method for the removal of environmentally hazardous NO_x emission from automotive engines [4]. From the extensive investigation so far, not only zeolite-based catalysts [7,8] but also metal oxide-based catalysts [9,10] were found to catalyze the NO reduction by hydrocarbons. Although a large number of catalysts systems have been investigated [4,7,10], no suitable catalyst has been found practical for this purpose. Zeolite-based catalysts, which were known to be very effective for NO reduction by hydrocarbons, are not promising candidates for practical use due to their instability under hydrothermal conditions [11]. On the other hand, the metal oxide catalysts, with hydrothermal stability higher than zeolites, have currently attracted much interest from researchers.

Ceria-based catalysts such as CeO_2 and CeO_2-ZrO_2 catalysts doped with precious or transition metal have been studied extensively for NO reduction by CO. CeO_2 is one of the important additives in the formulation of three-way catalysts. Its key roles include water gas shift reaction, dispersion of precious metals as well as inhibition of the sintering of alumina support [12]. By comparison, ZrO_2 has better thermal stability and sulphur resistance [13]. Di Monte et al. [14] reported that $Pd/Ce_{0.6}Zr_{0.4}O_2/Al_2O_3$ catalyst system showed a very high activity for NO reduction by CO below 500 K. They attributed the high activity to a promoting effect of the $CeO_{0.6}Zr_{0.4}O_2$ on the NO conversion. Similar result has been observed over Rh/CeO_2-ZrO_2 catalyst [15], where they reported that the NO reduction occurred at the Ce^{3+} sites on the catalyst to give N_2 and N_2O. A lot of research works have reported that CeO_2-ZrO_2-based catalysts showed good activity in the NO + CO reaction [16,17], but relatively little studies on SCR of NO by hydrocarbons over CeO_2-ZrO_2-based catalysts exist in the literature. Thus, extended studies should be carried out over these catalysts, as the catalysts may be suitable for SCR of NO by hydrocarbon in the presence of excess O_2.

The idea of combining two metals on a supported catalyst to increase the interaction of hydrocarbons and NO_x stimulated by the different active catalytic sites was proposed recently [18]. The bimetallic zeolite-based catalytic systems have been extensively examined for SCR of NO_x using hydrocarbon [19,20]. Regrettably, these catalysts are unpromising for practical application due to their poor sulphur and water tolerances [21]. Therefore, the metal oxide supported bimetal catalyst is deliberated as a potential candidate for SCR-HC. For example, we have reported that both $Cu/Cr/CeO_2$ [22] and $Cu/Ag/CeO_2$ [23] showed higher activity than Cu/CeO_2 and Ag/CeO_2. Furthermore, the activity of NO reduction was also enhanced by the addition of Cs to Ag/Al_2O_3 catalyst in the presence of SO_2 [24].

In our previous study [23], we reported that the reduction of NO under lean-burn condition at 400 °C was greatly enhanced by the addition of Cu and Ag on the CeO_2 catalyst. In present work, we attempt to investigate the catalytic performances of CeO_2-ZrO_2 catalyst doped with Cu and Ag in the selective reduction of NO by C_3H_6 in the presence of excess O_2. The effects of the incorporation of ZrO_2 on the catalytic performance of CeO_2-ZrO_2 catalysts in the SCR-HC are discussed in this paper. Furthermore, the effects of process parameters (reaction temperature, NO concentration and C_3H_6 concentration) on the catalytic performance of the catalyst were studied using design of experiments (DOE). The central composite design (CCD) coupled with response surface methodology (RSM) was utilized to predict the optimum values of process parameters for maximum NO conversion. Finally, the effect of large concentration of water vapor (10%) on the catalytic activity of the catalyst was also investigated.

2. Experimental

2.1. Catalyst preparation

The CeO_2 and ZrO_2 support were prepared by thermal decomposition of $Ce(NO_3)_3{\cdot}6H_2O$ (Acros Organics, 99.5%) and $ZrO(NO_3)_2{\cdot}7H_2O$ (Acros Organics, 99.5%), respectively, at 650 °C for 5 h as reported by de Leitenburg et al. [25]. The mixed oxide CeO_2-ZrO_2 was prepared by co-precipitation from an aqueous solution of $Ce(NO_3)_3{\cdot}6H_2O$ and $ZrO(NO_3)_2{\cdot}7H_2O$ in the required proportions through hydrolysis with aqueous NH_3. The precipitate was centrifuged, washed several times with distilled water, and then dried at 110 °C overnight, followed by calcination at 650 °C for 5 h. The support catalysts are denoted as CeO_2(*a*)-ZrO_2(*b*), where (*a*) represents the weight percent of CeO_2 and (*b*) denotes the weight percent of ZrO_2 in the catalysts.

The co-impregnation method was employed to synthesize the Cu and Ag doubly promoted CeO_2 catalysts. In this case, the required amounts of $Cu(NO_3)_2{\cdot}3H_2O$ (Emory, 99.0%) and $AgNO_3$ (R & M Chemicals, 99.5%) aqueous solutions were simultaneously impregnated with the CeO_2 catalyst support. Subsequently, the resulting solution was stirred for 17 h at room temperature and then dried in the oven at 110 °C overnight, followed by calcinations at 550 °C for 5 h to decompose the nitrate species present in the catalysts. The catalysts are denoted as Cu(*x*)/Ag(*y*)/CeO_2, where (*x*) represents the weight percent of Cu and (*y*) denotes the weight percent of Ag in the catalysts. The Cu and Ag doubly promoted CeO_2-ZrO_2 catalysts were prepared similar to the preparatory methods for $Cu/Ag/CeO_2$ catalyst.

2.2. Catalyst characterization

The XRD patterns, acquired using a Siemen D5000 employing Cu Kα radiation (λ = 1.54056 Å, 40 kV, 30 mA), was used to determine the crystallinity and phase purity of the samples. The XRD patterns were recorded in the 2θ range of 5–80°, with a scan speed of 0.05° s^{-1}. The average crys-

tallite size was determined from the line widths of the XRD peaks corresponding to (1 1 1) reflection, using the Scherrer equation.

The BET surface area was estimated from the N_2 adsorption isotherms, which were obtained at liquid nitrogen temperature (−196 °C) with an ASAP 2000 Micromeritics Analyser, utilizing a static volumetric technique. Nitrogen was of 99.9995% purity. The specific surface area was determined from the linear portion of the BET plot. Prior to the determination of the isotherm, the dried catalysts (0.3–0.4 g) were degassed for 16 h at 220 °C under a residual pressure of 1 Pa in order to remove moisture.

Temperature-programmed reduction (TPR) experiments were performed using a Micromeritics 2900 TPD/TPR equipped with a thermal conductivity detector. For the H_2 reduction analysis, 0.05 g of catalyst was used and treated by 10% of H_2 in argon at 50 ml min^{-1}. The temperature was raised from 100 to 950 °C at a heating rate of 10 °C min^{-1}.

2.3. Catalytic activity measurement

Catalytic activity measurements were carried out in a flow apparatus by using a lab-scale fixed bed reactor (Stainless Steel 316) with inner diameter 10 mm and length 300 mm. Prior to the reaction, one gram of the synthesized catalyst, supported on ceramic wool, was loaded into the reactor. The catalyst was pretreated using helium gas at 500 °C for 1 h. After the preheating period, the reactant gas mixtures comprising of 2000 ppm NO (B.O.C. special gases, 99.5% purity), 2000 ppm C_3H_6 (B.O.C. special gas, 99% purity), 10% O_2 (Malaysian Oxygen Bhd., 99.80%), 0% water vapor (if present) and balance He (Air Products, 99.999% purity) were fed into the reactor. The total gas flow rate was 500 ml min^{-1} (F/W = 30,000 ml g-cat.$^{-1}$ h^{-1}). The total gas flow rate employed in this research work was confirmed to be in the reaction-limited regime by measuring the NO conversion versus F/W curve. When water was added into the reactor through a water pump, all the lines were heated using heating tape, which were connected to a temperature controller, to above 120 °C to prevent condensation of water. Water contained in the outlet stream was removed in a condenser before the gas composition analysis in order to protect the GC columns from water. The reaction temperature controlled by a temperature-programmed reactor furnace (Carbolite® VST 12/30/200) was increased from 250 to 550 °C in steps of 50 °C. The concentration of NO was analyzed with a NO_x emission analyzer (Bacharach NONOXOR® II). The compositions of other products were analyzed by using a gas chromatograph (Agilent 6890 Series) equipped with a TCD detector. The concentrations of CO_2 and C_3H_6 were analyzed by a Porapak N column, while a Molecular Sieve 5A column was used for the analysis of N_2 and CO. The reaction results were evaluated in terms of NO conversion, C_3H_6 conversion and competitiveness factor ($S_{SCR\text{-}HC}$). The $S_{SCR\text{-}HC}$ was evaluated by calculating the ratio between oxygen atoms supplied from NO and all oxygen atoms react with hydrocarbons to form CO and CO_2 [22,23] as in Eq. (1). It gives a measure of the ability of the hydrocarbon species to be oxidized by NO rather than by O_2.

$$S_{SCR\text{-}HC}\,(\%) = \frac{2[N_2]}{2[CO] + 3[CO_2]} \times 100\% \quad (1)$$

where $[N_2]$, $[CO]$ and $[CO_2]$ are expressed as molar flow rates. The $S_{SCR\text{-}HC}$ is equal to 100% if the hydrocarbon is completely oxidized by NO. It decreases upon increase in the hydrocarbon oxidation rate.

3. Results and discussion

3.1. Catalyst characterizations

3.1.1. X-ray diffraction (XRD) and BET surface area

Fig. 1 shows the XRD patterns of CeO_2, CeO_2(75)-ZrO_2(25), CeO_2(50)-ZrO_2(50), CeO_2(25)-ZrO_2(75), Cu(4)/

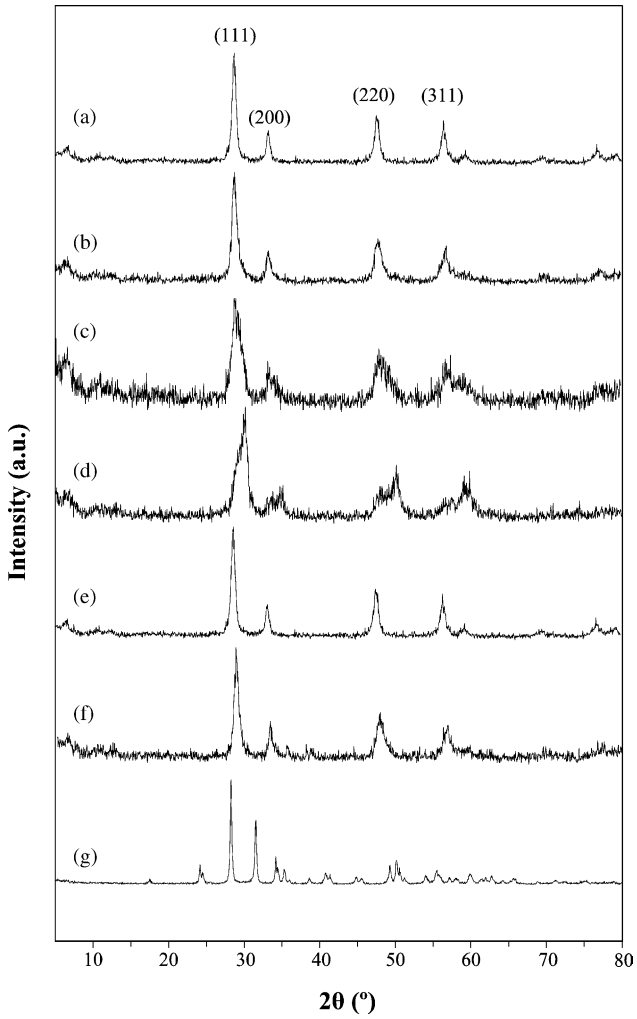

Fig. 1. XRD patterns of catalysts: (a) CeO_2, (b) CeO_2(75)-ZrO_2(25), (c) CeO_2(50)-ZrO_2(50), (d) CeO_2(25)-ZrO_2(75), (e) Cu(4)/Ag(1)/CeO_2, (f) Cu(4)/Ag(1)/CeO_2(75)/ZrO_2(25) and (g) ZrO_2.

$Ag(1)/CeO_2$, $Cu(4)/Ag(1)/CeO_2(75)$-$ZrO_2(25)$ and ZrO_2 catalysts. Pure CeO_2 catalyst (curve a) displayed the XRD patterns corresponding to the distinct, cubic, fluorite structure with intense bands at about 28.6°, 33.1°, 47.5° and 56.4° which represent the indices of (1 1 1), (2 0 0), (2 2 0) and (3 1 1) planes, respectively [26–28]. The XRD pattern of $CeO_2(75)$-$ZrO_2(25)$ (curve b) catalyst is similar to that of pure CeO_2 and no additional peaks attributed to tetragonal ZrO_2 (curve g) were observed, indicating that ZrO_2 was incorporated into the CeO_2 lattice to form solid solution and sustaining the fluorite structure. As can be seen from Fig. 1, the shift of the ceria peaks for CeO_2-ZrO_2-based catalysts to higher 2θ values compared to CeO_2 is evidence of an insertion of smaller Zr^{4+} ions in the lattice of CeO_2 [29]. With the loading of 25 wt% Zr in the CeO_2, the ceria peaks that was originally at 2θ of 28.6° and 33.1° was shifted slightly to 29.0° and 33.5°, respectively. As the Zr content increased to 75 wt%, the shift of ceria peak became significant, from 2θ of 28.6° to 30.0° which overlapped with a ZrO_2 line at 30.1°. Besides, a new peak at 2θ of 34.5° which is closed to the tetragonal ZrO_2 line (curve g) was detected. These observations indicate the formation of tetragonal structure in the CeO_2-ZrO_2-based catalysts with high Zr content [30]. As compared with the XRD patterns of CeO_2 and $CeO_2(75)$-$ZrO_2(25)$ catalysts, the XRD peaks observed for $CeO_2(50)$-$ZrO_2(50)$ and $CeO_2(25)$-$ZrO_2(75)$ catalysts were more broader. This broadening further confirmed the distortion of cubic phase of fluorite structure to a tetragonal structure due to the incorporation of high Zr content into CeO_2 [31].

The crystallite sizes of CeO_2-ZrO_2-based catalysts were estimated from the X-ray linewidths of the peaks corresponding to (1 1 1) using the Scherrer equation. The dimension of CeO_2-ZrO_2 crystallites were in the range of 5.9–13.4 nm. The crystallite sizes of the supported oxide species decreased with increasing Zr content. The observation is in accordance with the BET surface area results shown in Table 1, where CeO_2-ZrO_2-based catalysts with higher Zr loading showed larger surface area than pure CeO_2 catalyst.

XRD peaks due to CuO, Cu_2O or Ag_2O, on the other hand, were not detected in the $Cu(4)/Ag(1)/CeO_2$ and $Cu(4)/Ag(1)/CeO_2(75)$-$ZrO_2(25)$ samples. The absence of CuO and Ag_2O peaks may be attributed to the Cu and Ag particles being too small to be detected and the well dispersion of these particles on the surface of the catalysts. The presence of Cu and Ag increased the crystallite size of ceria for both the $Cu(4)/Ag(1)/CeO_2$ and $Cu(4)/Ag(1)/CeO_2(75)$-$ZrO_2(25)$ catalysts. The increase is more significant on the $Cu(4)/Ag(1)/CeO_2$ catalyst where the crystallite size of ceria increased from 12.5 nm (for pure CeO_2) to 18.3 nm (for $Cu(4)/Ag(1)/CeO_2$). In contrast, the increase in the crystallite size of ceria for $Cu(4)/Ag(1)/CeO_2(75)$-$ZrO_2(25)$ catalyst is not very obvious, only from 11.0 nm (for pure $CeO_2(75)$-$ZrO_2(25)$) to 12.1 nm (for $Cu(4)/Ag(1)/CeO_2(75)$-$ZrO_2(25)$). At the same time, as shown in Table 1, the $Cu(4)/Ag(1)/CeO_2$ catalyst showed a noticeable decrease in the surface area, from 19.2 $m^2\,g^{-1}$ (for pure CeO_2) to 14.9 $m^2\,g^{-1}$ (for $Cu(4)/Ag(1)/CeO_2$). On the other hand, the decrease of surface area is not significant on the $Cu(4)/Ag(1)/CeO_2(75)$-$ZrO_2(25)$ catalyst. Combining the crystallite size and BET surface area data, we can suggest that the Cu and Ag species are more uniformly dispersed on the $Cu(4)/Ag(1)/CeO_2(75)$-$ZrO_2(25)$ catalyst due to its smaller crystallite ceria size and larger surface area than the $Cu(4)/Ag(1)/CeO_2$ catalyst.

3.1.2. Temperature-programmed reduction by H_2 (H_2-TPR)

The TPR-H_2 profiles for CeO_2, CeO_2-ZrO_2 with various Zr loading, $Cu(4)/Ag(1)/CeO_2$ and $Cu(4)/Ag(1)/CeO_2(75)$-$ZrO_2(25)$ catalysts are illustrated in Fig. 2. The reduction profile of the CeO_2 support is characterized by a single peak at about 756 °C. All the CeO_2-ZrO_2-based catalysts also show the peak at adjacent reduction temperature. Thus, it is reasonable to attribute this peak to the reduction of the CeO_2 since pure ZrO_2 is not reduced in H_2 in the temperature range 100–900 °C (not shown). As shown in Fig. 2, the incorporation of Zr to CeO_2 remarkably shifted H_2 consumption peak to lower temperatures compared to that of CeO_2 (curves b–d). However, it should be noted that the H_2 consumption peak of the CeO_2-ZrO_2 mixed oxides shifted to higher temperatures with increasing Zr content from 25 to 75 wt%. According to XRD patterns and TPR results, one can speculate $CeO_2(75)$-$ZrO_2(25)$ with mainly cubic phase is more easier to reduce than the $CeO_2(50)$-$ZrO_2(50)$ and $CeO_2(25)$-$ZrO_2(75)$ catalysts that are dominated by tetragonal phase. This observation is in accordance with that reported by Fornasiero et al. [31] and Thammachart et al. [32] where high Zr content in the CeO_2-ZrO_2 catalyst will result in the formation of irreducible structure of the material.

Table 1
Summary of results from XRD and NA

Sample	BET surface area ($m^2\,g^{-1}$)	Pore volume ($cm^3\,g^{-1}$)	Average pore diameter (nm)	Crystallite size[a] (nm)
CeO_2	19.2	0.00038	8.9	13.4
$CeO_2(75)$-$ZrO_2(25)$	27.5	0.00089	9.4	11.0
$CeO_2(50)$-$ZrO_2(50)$	31.2	0.00125	11.3	6.3
$CeO_2(25)$-$ZrO_2(75)$	40.2	0.00212	15.8	5.9
$Cu(4)/Ag(1)/CeO_2$	14.9	0.00033	8.2	18.3
$Cu(4)/Ag(1)/CeO_2(75)$-$ZrO_2(25)$	26.5	0.00132	9.0	12.1

[a] Calculation form the peak at 28.6° in the XRD pattern using the Scherrer equation.

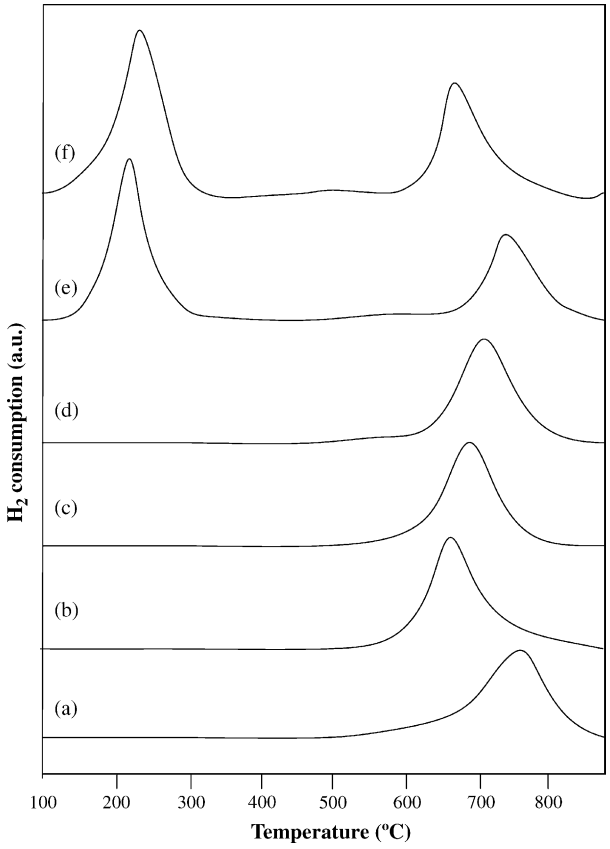

Fig. 2. TPR-H_2 profiles for (a) CeO_2, (b) CeO_2(75)-ZrO_2(25), (c) CeO_2(50)-ZrO_2(50), (d) CeO_2(25)-ZrO_2(75), (e) Cu(4)/Ag(1)/CeO_2 and (f) Cu(4)/Ag(1)/CeO_2(75)/ZrO_2(25).

The presence of 4 wt% Cu and 1 wt% Ag strongly modifies the TPR profiles of the pure CeO_2 and CeO_2(75)-ZrO_2(25) catalysts. Low temperature reduction peaks at 225 and 235 °C were observed over Cu(4)/Ag(1)/CeO_2 and Cu(4)/Ag(1)/CeO_2(75)-ZrO_2(25) catalysts, respectively, instead of the peak corresponding to reduction of CeO_2 at higher temperature. It has been reported in previous literatures on Cu/TiO_2 and Cu/ZrO_2 [33,34] that the reduction peak at around 220 °C can be assigned to the reduction of Cu^{2+} species to Cu^0 and indicates the presence of highly dispersed Cu^{2+} species. The lack of peaks at temperature lower than 200 °C which is attributed to the reduction of oxocations $(Cu–O–Cu)^{2+}$ [35,36] enable us to attribute the reduction peaks at 225 and 235 °C to the presence of highly dispersed Cu^{2+} ions on these catalysts. In addition, these reduction peaks could also be assigned to the reduction of Ag_2O since it has been reported that the combination of Cu with Ag generally produced a single reduction peak at 254 °C [23] and 327 °C [37]. The difference in the reduction temperature between Cu(4)/Ag(1)/CeO_2 and Cu(4)/Ag(1)/CeO_2(75)-ZrO_2(25) catalysts can be attributed to the interaction between the metal and support. According to Chien et al. [38], the strong metal-support interaction generally leads to an increase in the reduction temperature. Therefore, we can deduce that Cu(4)/Ag(1)/CeO_2(75)-ZrO_2(25) catalyst possesses stronger metal-support interaction than Cu(4)/Ag(1)/CeO_2 catalyst.

3.2. Catalytic performance over CeO_2-ZrO_2-based catalysts

Fig. 3 shows the NO and C_3H_6 conversion achieved over CeO_2-ZrO_2 catalysts with Zr content ranging from 25 to 75 wt%. The addition of Zr onto CeO_2 greatly enhanced the NO conversion and exhibited higher catalytic activity than pure CeO_2 and pure ZrO_2. One can claim that the incorporation of Zr into CeO_2 lattices to form solid solution promoted the reduction of NO over these catalysts. The optimal Zr loading is found to be 25 wt% with NO reduction of 29%. Further increases in Zr content definitely reduce the NO conversion. The favorable effect of the addition of small amount of Zr on the catalytic activity of the CeO_2(75)-ZrO_2(25) catalyst can be attributed to its structural property. Based on the structures as revealed by the XRD results, it can be said that the cubic-fluorite structure of CeO_2(75)-ZrO_2(25) catalyst is more active than tetragonal structure of CeO_2(50)-ZrO_2(50) and CeO_2(25)-ZrO_2(75). Hori et al. [39] observed that the optimum Zr concentration was around 25% for the $Ce_nZr_{1-n}O_2$ samples prepared by co-precipitation of hydroxides. They found that the beneficial effects of ZrO_2 were pronounced in solid solutions which had the oxygen storage capacity values three to five times higher than that of pure CeO_2. Numerous studies have reported that CeO_2-ZrO_2 mixed oxides have the ability to easily remove bulk oxygen species at moderate temperatures. ZrO_2 is associated with its ability to modify the oxygen sub-lattice in the CeO_2-ZrO_2 mixed oxides and typically regarded to contribute to the improvement of the lattice space, therefore facilitating the migration of oxygen atoms [40]. By using the CeO_2-ZrO_2 mixed oxides the catalysts is more effective due to the high oxygen mobility in the bulk and the lattice oxygen species can effectively participate in the redox processes [40]. Furthermore, the redox properties of CeO_2 have been enhanced

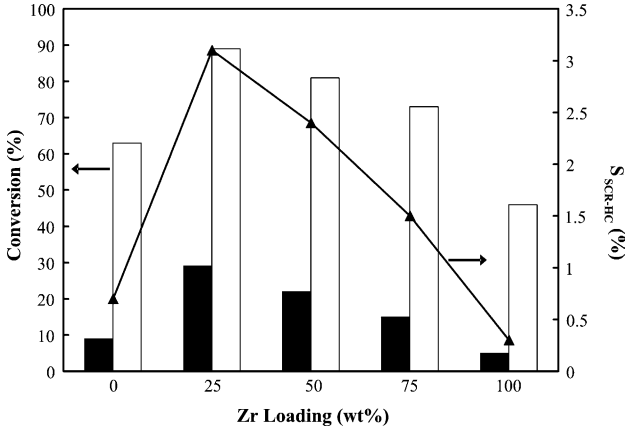

Fig. 3. Effect of Zr loading on NO conversion (■), C_3H_6 conversion (□) and $S_{SCR\text{-}HC}$ (▲) at 400 °C (reaction conditions: 2000 ppm NO, 2000 ppm C_3H_6, 10% O_2 with balance of He, F/W = 30,000 ml g-cat.$^{-1}$ h^{-1}).

by the addition of Zr^{4+} into the lattice of CeO_2 by the formation of solid solutions [31]. Ranga Rao et al. [15] reported that NO is effectively decomposed at the Ce^{3+} sites in the Rh- and Pt-loaded Ce-containing materials, suggesting a direct participation of the reduced support in the NO conversion. It was also observed that upon incorporation of ZrO_2 into a solid solution with CeO_2, the reducibility of the Ce^{4+} is strongly enhanced compared to pure CeO_2 both in the unsupported and metal-loaded samples.

Among the CeO_2-ZrO_2-based catalysts investigated for SCR of NO by C_3H_6, CeO_2(75)-ZrO_2(25) catalyst demonstrated the highest $S_{SCR\text{-}HC}$ and C_3H_6 conversion. The results indicated that CeO_2(75)-ZrO_2(25) catalyst with low Zr loading has the ability to activate C_3H_6 for selectively reducing NO in the presence of excess O_2. Although the C_3H_6 conversions achieved over the CeO_2(50)-ZrO_2(50) and CeO_2(25)-ZrO_2(75) catalysts can be considered high, their $S_{SCR\text{-}HC}$ values were rather low. It seems that the C_3H_6 activation effect has accelerated the side reaction of C_3H_6 combustion by O_2, and at the same time decreased the amount of C_3H_6 available to selectively reduce NO over these catalysts.

In order to elucidate the effect of NO on the C_3H_6 conversion of the catalysts, extended investigation was conducted over the catalytic activity for direct oxidation of C_3H_6 with O_2. Fig. 4 compares C_3H_6 conversion data between $NO + C_3H_6 + O_2$ and $C_3H_6 + O_2$ reaction at 400 °C over the CeO_2-ZrO_2-based catalysts. For comparison, the reaction conditions for $C_3H_6 + O_2$ reaction remained the same as that in the $NO + C_3H_6 + O_2$ reaction. It is clear that the C_3H_6 conversion over the CeO_2 and ZrO_2 catalysts in the $C_3H_6 + O_2$ reaction is almost the same as that in the $NO + C_3H_6 + O_2$ reaction. In contrast, the C_3H_6 conversions over all the CeO_2-ZrO_2 catalysts were much higher for $NO + C_3H_6 + O_2$ reaction than those for $C_3H_6 + O_2$ reaction, signifying the presence of NO promotes the oxidation of C_3H_6 over these catalysts. The increase of C_3H_6 conversion in the presence of NO is more obvious on the CeO_2(75)-ZrO_2(25) catalyst as depicted in Fig. 4. These results again reveal that the presence of Ce and Zr in the catalysts enhance the capability of C_3H_6 to selectively reduce NO in the presence of excess O_2 especially for CeO_2(75)-ZrO_2(25) catalyst and are consistent with the $S_{SCR\text{-}HC}$ values.

Although CeO_2(75)-ZrO_2(25) catalyst has lower surface area than CeO_2(50)-ZrO_2(50) and CeO_2(25)-ZrO_2(75) catalysts, it exhibited the highest catalytic activity for NO reduction. The result suggests that the NO reduction is almost independent of surface area. The difference between the catalytic performances of the CeO_2-ZrO_2-based catalysts can be associated with their reducibility as shown in Fig. 2. It was found that the CeO_2(75)-ZrO_2(25) catalyst with the highest NO reduction activity is more reducible than CeO_2(50)-ZrO_2(50) and CeO_2(25)-ZrO_2(75) catalysts. On the basis of the H_2-TPR profiles and catalytic results, high reducibility was presumed to grant the promising performance of CeO_2(75)-ZrO_2(25) catalyst by activating C_3H_6 to selectively reduce NO.

3.3. Catalytic performance over Cu(4)/Ag(1)/CeO_2 and Cu(4)/Ag(1)/CeO_2(75)-ZrO_2(25)

In order to elucidate the effect of the presence of Zr on the catalytic performance of the catalysts, we compared the NO and C_3H_6 conversion over the Cu(4)/Ag(1)/CeO_2 and the Cu(4)/Ag(1)/CeO_2(75)-ZrO_2(25) catalysts, and the results are shown in Fig. 5. Similar trends were observed irrespective of the supports. Volcano-type NO conversion versus temperature curves were obtained and complete C_3H_6 conversion was achieved at the temperature where the maximum NO conversion was measured over both catalysts. The differences between both catalysts are the maximum NO conversion improved from 82% to 89% and the temperature of maximum NO conversion shifted to lower value with the addition of ZrO_2 to the support of the catalyst. Furthermore, the Cu(4)/Ag(1)/CeO_2(75)-

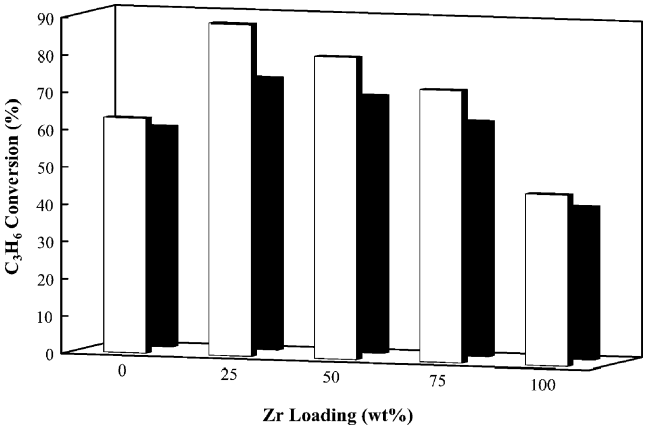

Fig. 4. C_3H_6 conversion of CeO_2-ZrO_2-based catalysts with various Zr loading in the presence (□) and absence (■) of NO at 400 °C (reaction conditions: 2000 ppm NO (if present), 2000 ppm C_3H_6, 10% O_2 with balance of He, F/W = 30,000 ml g-cat.$^{-1}$ h^{-1}).

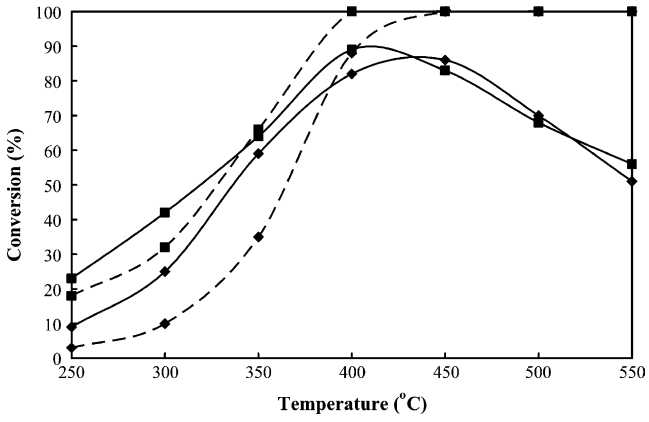

Fig. 5. Conversion of NO (solid line) and C_3H_6 (dashed line) vs. temperature over (♦) Cu(4)/Ag(1)/CeO_2 and (■) Cu(4)/Ag(1)/CeO_2(75)-ZrO_2(25) (reaction conditions: 2000 ppm NO, 2000 ppm C_3H_6, 10% O_2 with balance of He, F/W = 30,000 ml g-cat.$^{-1}$ h^{-1}).

ZrO_2(25) catalyst showed wider operating temperature window (300–550 °C) for NO conversion; more than 50% compared to Cu(4)/Ag(1)/CeO_2 catalyst. As depicted in Fig. 5, the Cu(4)/Ag(1)/CeO_2(75)-ZrO_2(25) catalyst exhibited higher C_3H_6 conversion than the Cu(4)/Ag(1)/CeO_2 catalyst at 300 and 350 °C. Consequently, the high NO conversion obtained over Cu(4)/Ag(1)/CeO_2(75)-ZrO_2(25) catalyst at low temperature can be attributed to the activation of C_3H_6 to react with NO.

In Table 2, it was found that the conversion of C_3H_6 in the NO + C_3H_6 + O_2 reaction was higher than that in the C_3H_6 + O_2 reaction over the Cu(4)/Ag(1)/CeO_2 and Cu(4)/Ag(1)/CeO_2(75)-ZrO_2(25) catalysts at 350 °C. The result reveals that the presence of NO actually promotes the C_3H_6 oxidation over these catalysts. Moreover, it is interesting to note that although Cu(4)/Ag(1)/CeO_2(75)-ZrO_2(25) catalyst exhibited higher NO conversion than Cu(4)/Ag(1)/CeO_2 catalyst, both catalysts attained nearly the same $S_{SCR\text{-}HC}$ values at 350 °C. The result implied that the addition of Zr has an effect of activating C_3H_6 to react with NO, but at the same time, the side reaction of C_3H_6 combustion also occur over this catalyst. In addition, it can be seen that the CO selectivity in the NO + C_3H_6 + O_2 reaction was higher than that in the C_3H_6 + O_2 reaction over the Cu(4)/Ag(1)/CeO_2 catalyst, suggesting that the partial oxidation of hydrocarbon occur over this catalyst in the presence of NO. Shimizu et al. [41] have reported that organic intermediates generated from the partial oxidation of hydrocarbon are very active to reduce NO in the lean condition, and this process is always accompanied by high rate of CO formation. Therefore, it can be concluded that partial oxidation of C_3H_6 is an important reaction step for SCR of NO over Cu(4)/Ag(1)/CeO_2 catalyst. However, the addition of Zr to the support of the Cu(4)/Ag(1)/CeO_2 catalyst generally lower the CO selectivity in the NO + C_3H_6 + O_2 reaction as shown in Table 2. The result strongly reflected that the CO oxidation to CO_2 was favored in the CeO_2-ZrO_2-based catalyst as demonstrated in previous literatures [32,42] and the CO concentration in the product stream was reduced.

The improvement of the catalytic activity of Cu(4)/Ag(1)/CeO_2(75)-ZrO_2(25) catalyst at the low temperature region (250–350 °C) can be ascribed to the strong metal-support interaction of the catalyst. It has been shown that in the XRD and NA characterizations that the catalyst had smaller ceria crystallite size and the larger surface area than the Cu(4)/Ag(1)/CeO_2 catalyst. These features may result in a larger interface between Cu and Ag species and the support, resulting in a strong metal-support interaction as evident in the TPR profiles. In addition, the high reducibility possessed by CeO_2-ZrO_2 support than that of CeO_2 support is believed to enhance the C_3H_6 activation at low temperature as discussed in previous section. Thus, NO can be selectively reduced by C_3H_6 at low temperature region over Cu(4)/Ag(1)/CeO_2(75)-ZrO_2(25) catalyst. Based on the above discussion, we can conclude that the strong metal-support interaction and high reducibility of the CeO_2-ZrO_2 support are responsible for the improvement of the NO conversion activity at low temperature.

3.4. Process variables study using central composite design

Design of experiments was carried out using STATISTICA Software Version 6 (Statsoft Inc.) to study the effect of operating variables over SCR of NO activity. The central composite design coupled with response surface methodology was employed to obtain the combination of values (NO concentration, C_3H_6 concentration and reaction temperature) that optimizes the response (NO conversion) and to determine the most influential variable that affects the value of response at fixed amount of catalyst (1 g Cu(4)/Ag(1)/CeO_2(75)-ZrO_2(25) catalyst) and F/W of 30,000 ml g-cat.$^{-1}$ h^{-1}. These three operating variables were chosen since these variables varied frequently in the engine operation. Besides, similar variables have been chosen by Bhatia and co-workers [43] in their recent work. Several other responses were also considered in the central composite design such as C_3H_6 conversion and $S_{SCR\text{-}HC}$.

According to central composite design, the total number of experiment combinations is $2^k + 2k + n_0$, where k is the number of independent variables and n_0 is the number of repetition of the experiments at the center point. The following equation is designed to estimate the coefficients of a quadratic model:

$$y = \beta_o + \sum_{i=1}^{k} \beta_i x_i + \sum_{i=1}^{k} \beta_{ii} x_i^2 + \sum \sum_{i<j} \beta_{ij} x_i x_j \quad (2)$$

where y is the predicted response, x_i the coded factor value, β_o the offset term, β_i the linear term, β_{ii} the squared term and

Table 2
Catalytic activity of Cu(4)/Ag(1)/CeO_2 and Cu(4)/Ag(1)/CeO_2(75)-ZrO_2(25) catalysts for C_3H_6 oxidation in the presence and absence of NO at 350 °C

Catalyst	C_3H_6 conversion (%)	CO selectivity (%)	$S_{SCR\text{-}HC}$ (%)
NO + C_3H_6 + O_2			
Cu(4)/Ag(1)/CeO_2	35	13	24.2
Cu(4)/Ag(1)/CeO_2(75)-ZrO_2(25)	66	5.3	23.6
C_3H_6 + O_2			
Cu(4)/Ag(1)/CeO_2	23	2.6	–
Cu(4)/Ag(1)/CeO_2(75)-ZrO_2(25)	45	1.5	–

Reaction conditions: 2000 ppm NO if present, 2000 ppm C_3H_6, 10% O_2 with balance of He, F/W = 30,000 ml g-cat.$^{-1}$ h^{-1}.

Table 3
The levels of independent variables in central composite design

Factor	Factor code	$-\alpha$	−1	0	+1	$+\alpha$
Reaction temperature (°C)	x_1	224	300	400	500	576
NO concentration (ppm)	x_2	818	1200	1700	2200	2582
C_3H_6 concentration (ppm)	x_3	818	1200	1700	2200	2582

Note: $-/+\alpha$, star point value; −1, low value; +1, high value; 0, center value.

β_{ij} is the interaction term. In this work, $n_0 = 2$ and $k = 3$ and therefore a total of 16 runs of experiments were needed to optimize the processing parameters for NO conversion. By substituting the value 3 for k, Eq. (2) becomes:

$$y = \beta_o + \beta_1 x_1 + \beta_2 x_2 + \beta_3 x_3 + \beta_{12} x_1 x_2 + \beta_{13} x_1 x_3 + \beta_{23} x_2 x_3 + \beta_{11} x_1^2 + \beta_{22} x_2^2 + \beta_{33} x_3^2 \quad (3)$$

The three independent variables in Eq. (3) were identified to be reaction temperature (x_1), inlet NO concentration (x_2) and inlet C_3H_6 concentration (x_3), while the response variable (y) was chosen to be NO conversion, C_3H_6 conversion or $S_{SCR\text{-}HC}$. The Statistica Software was utilized to estimate the relationship between the response variable and the independent variables in Eq. (3). Table 3 presents the factors and their design levels while Table 4 shows the experimental data of the three response variables for the 16 experiments. The α in Table 3 represents the distance from the center of the design space to a star point. The star points represent new extreme values (low and high) for each factor in the design. The precise value of α depends on certain properties desired for the design and on the number of factors involved. To maintain rotatability, the value of α depends on the number of experimental runs in the factorial portion of the central composite design. If the factorial is a full factorial, then:

$$\alpha = [B]^{1/4} \quad (4)$$

where B is the number of factorial runs (2^k, k = number of factors).

The statistical significance of the quadratic model (Eq. (3)) was checked by an F-test (ANOVA) with 95% degree of confidence.

3.4.1. NO conversion

The quadratic model for the NO conversion is presented in Eq. (5) as:

$$\text{NO conversion} = 81.70 + 4.98x_1 + 0.01x_2 + 2.79x_3 - 2x_1x_2 + 2x_1x_3 + 6x_2x_3 - 17.17x_1^2 - 4.31x_2^2 - 5.60x_3^2 \quad (5)$$

The ANOVA table displaying the total, regression and error of sum of square for NO conversion model is shown in Table 5. The F-value is a measurement of variance of data about the mean, based on the ratio of mean square of group variance due to error [44]. In general, if the model is a good prediction of the experimental results and the estimated factor effects are real, the calculated F-value should be several times larger than the tabulated value. In this study, the computed F-value for NO conversion model is bigger than the tabulated F-value ($F_{0.05} = 3.37$) at $\alpha = 0.05$ in the statistic table, it can be concluded that Eq. (5) gives good prediction of the NO conversion and the model was significant at a high confidence level.

Table 4
Central composite design and experimental results

Run	Manipulated variables			Responses		
	Reaction temperature (°C)	NO concentration (ppm)	C_3H_6 concentration (ppm)	NO conversion (%)	C_3H_6 conversion (%)	$S_{SCR\text{-}HC}$ (%)
1	300	1200	1200	51	38	25
2	300	1200	2200	39	22	21
3	300	2200	1200	48	49	29
4	300	2200	2200	56	65	33
5	500	1200	1200	61	98	6
6	500	1200	2200	53	91	5
7	500	2200	1200	46	100	8
8	500	2200	2200	66	100	7
9	400	1700	1700	81	86	21
10	224	1700	1700	20	11	36
11	576	1700	1700	42	100	3
12	400	818	1700	74	81	16
13	400	2582	1700	68	96	12
14	400	1700	818	58	90	10
15	400	1700	2581	76	83	18
16	400	1700	1700	83	87	21

Table 5
ANOVA results for the NO conversion models[a]

Source	Sum of squares (S.S.)	Degree of freedom	Mean squares	*F*-value
S.S. regression	4414.39	9	490.49	14.52
S.S. error	202.68	6	33.78	
S.S. total	4617.07	15		

[a] Determinant coefficient, $R^2 = 0.9527$.

Fig. 6 depicts the Student's *t*-distribution values in a Pareto chart and the corresponding *p*-values of the variables in Eq. (5). The *p*-value serves as a tool to determine the significance of each coefficient. The low values of *p*-value of less than 0.05 indicate the corresponding variables are more significant. As illustrated in Fig. 6, the independent variables such as reaction temperature and C_3H_6 concentration (x_1, x_1^2, x_3^2) had a significant effect on the NO conversion, especially reaction temperature (x_1^2) with a *p*-value of 0.000076. In addition, the interaction between NO concentration and C_3H_6 concentration (x_2x_3) could also be regarded as a significant factor in affecting the NO conversion with a *p*-value of 0.0266. The rest of the variables could be considered to be less significant to affect the NO conversion since their *p*-values are more than 0.05.

To investigate the effects of reaction temperature, NO and C_3H_6 concentrations on NO reduction, the three-dimensional contour plot was used to represent the regression model of Eq. (5) in Figs. 7 and 8. These figures clearly show that the reaction temperature has the most significant effect on the NO reduction compared to NO and C_3H_6 concentrations. As shown in Fig. 7, the NO conversion profiles as a function of reaction temperature show a volcano shape curve regardless of the NO concentration applied. The conversion of NO started at 250 °C, reached a maximum around 400 °C and then declined. The decrease of NO conversion at higher temperature (>450 °C) may be due to the rapid oxidation of C_3H_6 by O_2 and thus reduce the amount of C_3H_6 to selectively react with NO. On the other hand, Fig. 8 shows the effects of NO and C_3H_6 concentrations on the NO conversion activity of Cu(4)/Ag(1)/CeO_2(75)-ZrO_2(25) catalyst. The NO conversion has substantially decreased upon increased in the NO concentration or C_3H_6 concentration above 2000 ppm. It is clearly seen that the decrement in NO conversion is more pronounced with higher NO concentration. This phenomenon may be interpreted by the inhibition of C_3H_6

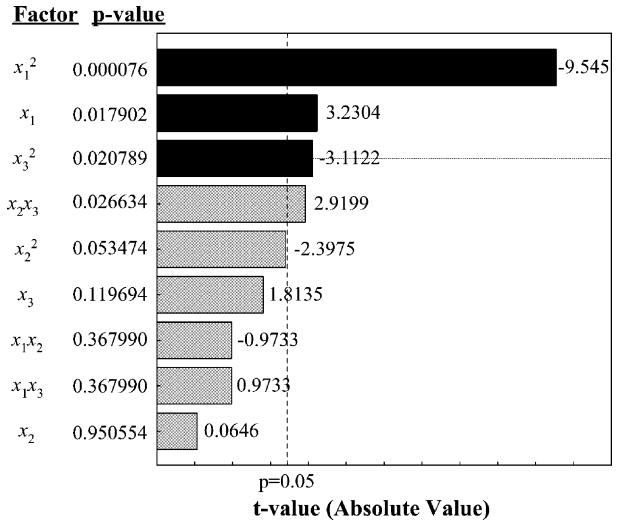

Fig. 6. Pareto chart of NO conversion.

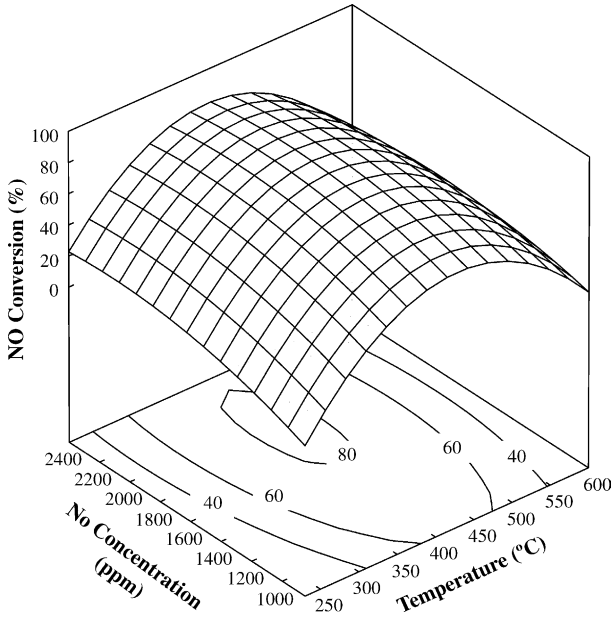

Fig. 7. The response surface plot of NO conversion as a function of reaction temperature (x_1) and NO concentration (x_2).

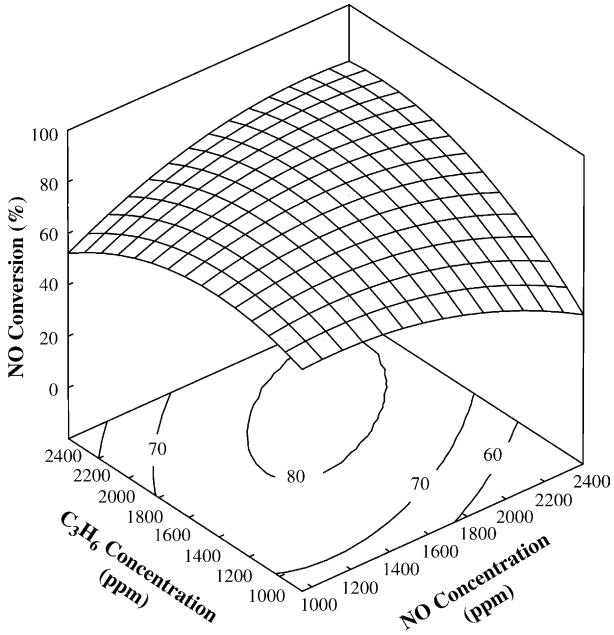

Fig. 8. The response surface plot of NO conversion as a function of NO concentration (x_2) and C_3H_6 concentration (x_3).

Table 6
ANOVA results for the C_3H_6 conversion models[a]

Source	Sum of squares (S.S.)	Degree of freedom	Mean squares	*F*-value
S.S. regression	11986.73	9	1366.626	26.21
S.S. error	312.90	6	52.15	
S.S. total	12299.63	15		

[a] Determinant coefficient, $R^2 = 0.9752$.

adsorption due to the large coverage of adsorbed nitrate species on the catalyst surfaces at high NO concentration, and hence, the amount of adsorbed C_3H_6 to react with NO is reduced.

3.4.2. C_3H_6 conversion

The quadratic model for the C_3H_6 conversion in term of the coded factors is represented as:

$$\begin{aligned} C_3H_6\ \text{conversion} = {} & 86.0977 + 26.1549x_1 + 6.0585x_2 \\ & - 1.3603x_3 - 5.3750x_1x_2 \\ & - 0.8750x_1x_3 + 4.8750x_2x_3 \\ & - 10.9987x_1^2 - 0.8737x_2^2 - 1.0344x_3^2 \end{aligned} \quad (6)$$

The computed *F*-value of the C_3H_6 conversion model in Table 6 is several times larger that the tabulated *F*-value, demonstrating that the present model is in good prediction of the experimental results. Fig. 9 shows the significance of each coefficient over the C_3H_6 model. The *p*-values in the Pareto chart imply that the coefficient for linear effect of reaction temperature (x_1), with a value of 0.00001, is the most significant. Besides, the coefficients for the quadratic effect of temperature (x_1^2) and the linear effect of NO concentration (x_2) may be significant to some extent, with a *p*-value of 0.0026 and 0.0195, respectively.

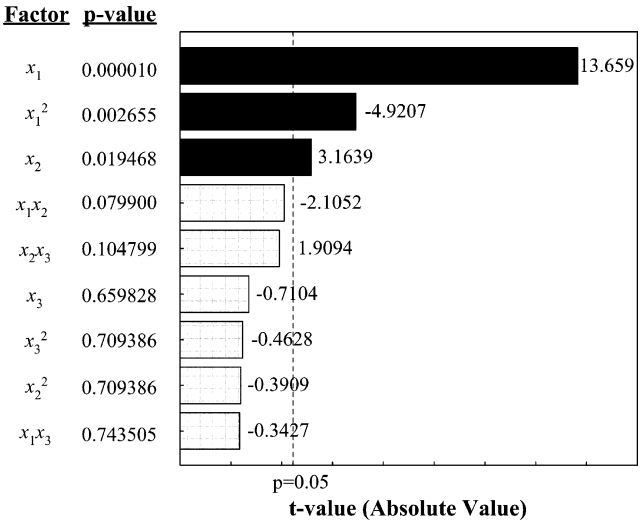

Fig. 9. Pareto chart of C_3H_6 conversion.

Table 7
ANOVA results for the $S_{SCR\text{-}HC}$ models[a]

Source	Sum of squares (S.S.)	Degree of freedom	Mean squares	*F*-value
S.S. regression	1526.89	9	169.654	12.55
S.S. error	81.122	6	13.520	
S.S. total	1608.012	15		

[a] Determinant coefficient, $R^2 = 0.9490$.

3.4.3. $S_{SCR\text{-}HC}$

An empirical relationship between $S_{SCR\text{-}HC}$ and coded factors is presented in Eq. (7):

$$\begin{aligned} S_{SCR\text{-}HC} = {} & 21.04659 - 9.85827x_1 + 0.91017x_2 \\ & - 0.85153x_3 - 1.5x_1x_2 - 0.25x_1x_3 + x_2x_3 \\ & - 0.36234x_1^2 - 2.13019x_2^2 - 2.13019x_3^2 \end{aligned} \quad (7)$$

The ANOVA table (Table 7) shows that the computed *F*-value was much greater than the tabulated *F*-value, further confirming that the model was significant at a high confidence level. It is also suggested from Fig. 10 that $S_{SCR\text{-}HC}$ was primarily determined by the linear term of reaction temperature and no significant effect exerted by the other two factors, which are NO and C_3H_6 concentrations.

The $S_{SCR\text{-}HC}$ model in Eq. (7) is shown graphically in Figs. 11 and 12. Figs. 11 and 12 depict that the $S_{SCR\text{-}HC}$ decreased as the temperature increased. At low temperature region (250–350 °C), high $S_{SCR\text{-}HC}$ values were attained, indicating that C_3H_6 was available in this temperature region to selectively reduce NO rather than be oxidized by O_2. However, further increase in the reaction temperature hastily reduced the $S_{SCR\text{-}HC}$ values. The results suggest the combustion process (C_3H_6 oxidation by O_2) became predominant in higher temperature region.

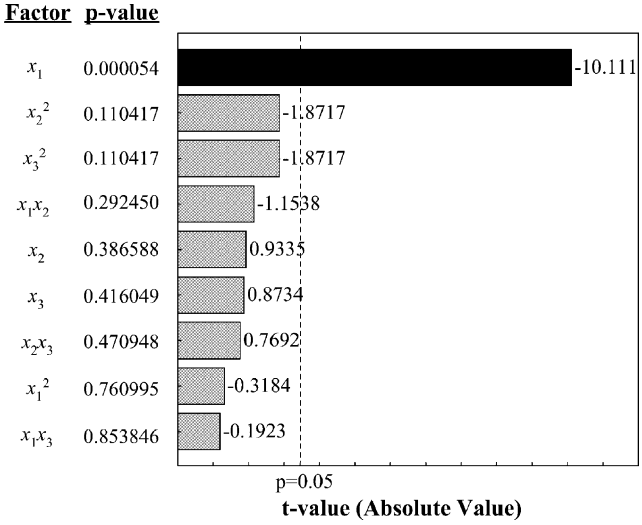

Fig. 10. Pareto chart of $S_{SCR\text{-}HC}$.

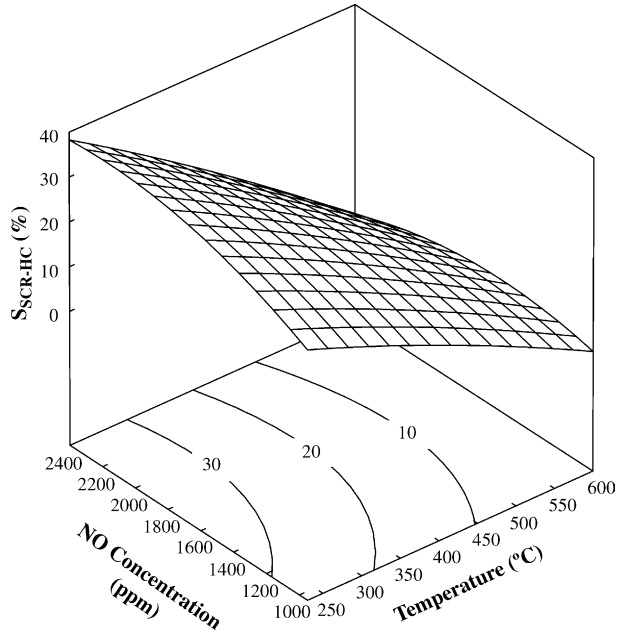

Fig. 11. The response surface plot of S_{SCR-HC} as a function of reaction temperature (x_1) and NO concentration (x_2).

3.4.4. Optimization of NO conversion using response surface methodology

From the response surface methodology by using Statistica Software, the predicted optimum NO conversion is found to be 82.89% at reaction temperature = 415.38 °C, NO concentration = 1827.16 ppm and C_3H_6 concentration = 1908.13 ppm with the corresponding S_{SCR-HC} value being 19.63%. To confirm these results, experimental rechecking was performed using the identical reaction temperature, NO and C_3H_6 concentrations. The NO conversion obtained from the experiment was 86.30% and the difference between the experimental and predicated NO conversion is 3.95%. The good correlation between these two results confirmed the validity of the response model and the model was proven to be adequate.

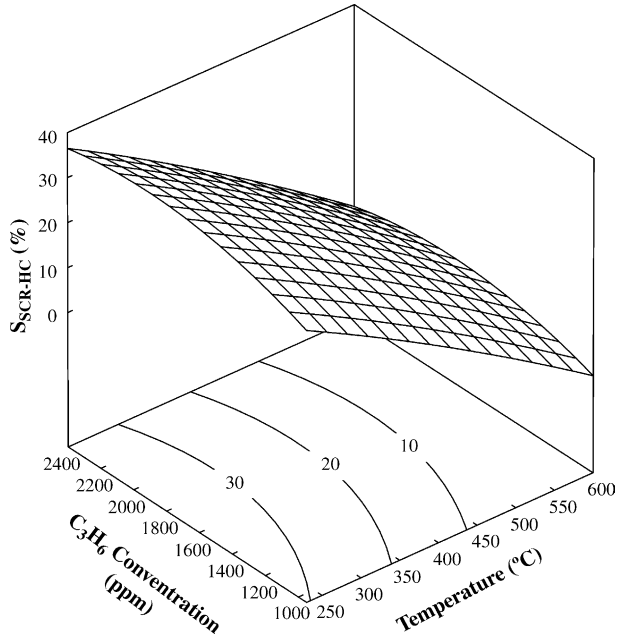

Fig. 12. The response surface plot of S_{SCR-HC} as a function of reaction temperature (x_1) and C_3H_6 concentration (x_3).

3.4.5. Effect of water vapor on the activity of Cu(4)/Ag(1)/CeO_2(75)-ZrO_2(25) for the SCR-HC of NO, as compared with Cu(4)/Ag(1)/CeO_2

Water vapor is one of the unavoidable components in exhaust gases which often cause deactivation of catalysts. Thus, resistance of SCR catalysts to deactivation by water vapor is very important for the practical demand of NO reduction. In this study, the effect of water vapor on the catalytic activity of Cu(4)/Ag(1)/CeO_2(75)-ZrO_2(25) catalyst was compared with that of Cu(4)/Ag(1)/CeO_2 catalyst under identical experiment conditions.

Fig. 13 compares the catalytic activities of Cu(4)/Ag(1)/CeO_2(75)-ZrO_2(25) and Cu(4)/Ag(1)/CeO_2 catalysts when water vapor was added to the reactant gases at 400 °C over a 3-h period. As can be seen in Fig. 13, the addition of 10% water vapor to the reactant gases inhibited the catalytic activity of the both catalysts. However, the inhibition effect was more pronounced over the Cu(4)/Ag(1)/CeO_2 catalyst. Catalyst deactivation by water vapor may probably be due to the competition between water vapor and C_3H_6 to adsorb on the same catalyst site. The lower adsorption enthalpy of light hydrocarbons such as C_3H_6 compared to water vapor is presumed to result in the C_3H_6 to be less adsorbed on the active sites to form the intermediate species for NO reduction following the addition of water vapor [45]. The NO conversions for the Cu(4)/Ag(1)/CeO_2(75)-ZrO_2(25) and Cu(4)/Ag(1)/CeO_2 catalysts decreased to 61% (from 88%) and 42% (from 81%), respectively. Therefore, it can be concluded that Cu(4)/Ag(1)/CeO_2(75)-ZrO_2(25) cat-

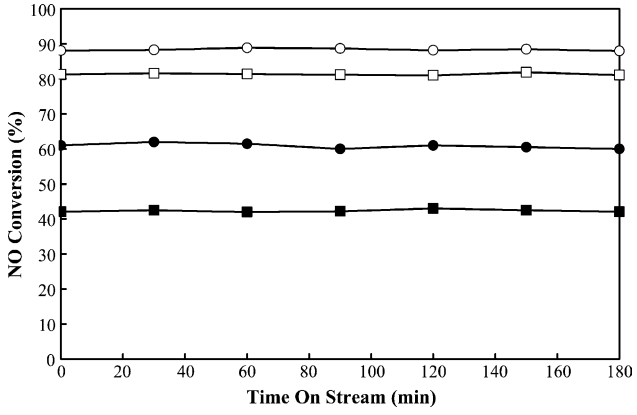

Fig. 13. Comparison of NO conversion activity between (□, ■) Cu(4)/Ag(1)/CeO_2 and (○, ●) Cu(4)/Ag(1)/CeO_2(75)-ZrO_2(25) catalysts in the absence and presence of H_2O. Open symbols (□, ○) indicate the results obtained in the absence of H_2O and the solid symbols (■, ●) in its presence (reaction conditions: 2000 ppm NO, 2000 ppm C_3H_6, 10% O_2, 10% H_2O (if present) with balance of He, F/W = 30,000 ml g-cat.$^{-1}$ h^{-1}).

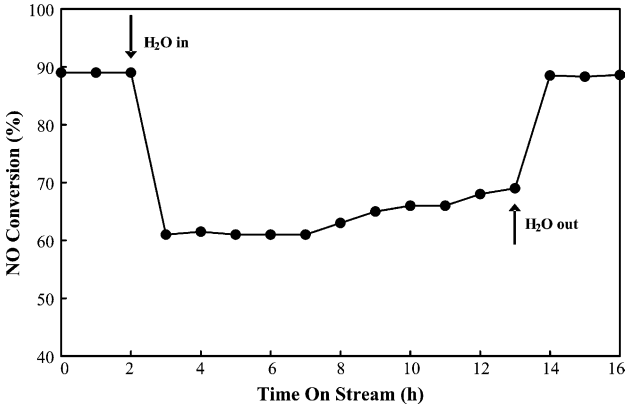

Fig. 14. Response of NO conversion over Cu(4)/Ag(1)/CeO_2(75)-ZrO_2(25) catalyst at 400 °C to the intermittent feed of 10% H_2O (reaction conditions: 2000 ppm NO, 2000 ppm C_3H_6, 10% O_2, 10% H_2O (if present) with balance of He, F/W = 30,000 ml g-cat.$^{-1}$ h^{-1}).

alyst exhibits higher resistance against water vapor in the reactant gases compared to Cu(4)/Ag(1)/CeO_2 catalyst. On the other hand, the large decrease of the performance of these catalysts can be attributed to the lighter alkene used in this study. Shimizu et al. [46] proposed that water had an inhibiting effect for the SCR with shorter alkanes than the octane due to the lower enthalpy of adsorption of lighter alkanes where the water and alkanes were competing for the adsorption sites.

Furthermore, Fig. 14 illustrates the response of the NO conversion over Cu(4)/Ag(1)/CeO_2(75)-ZrO_2(25) catalyst at 400 °C to the intermittent feed of 10% water vapor for SCR of NO by C_3H_6. The activity decreased as the water vapor was introduced but immediately recovered as soon as the water vapor was excluded from the reactant gases. The results indicated that the inhibition of water vapor over the catalytic performance of the Cu(4)/Ag(1)/CeO_2(75)-ZrO_2(25) catalyst was reversible and further confirmed that there was a competitive absorption between water vapor and C_3H_6 for the same catalyst site. In addition, it was interesting to observe that the activity of the Cu(4)/Ag(1)/CeO_2(75)-ZrO_2(25) catalyst did not decrease after 10 h on wet stream but appeared to slightly increase with time on stream as shown in Fig. 14. Similar observations were also revealed in previous literatures on Sn/Al_2O_3 [47] and Ga_2O_3-Al_2O_3 [48] catalysts. Haneda et al. [48] therefore proposed that one of the effects of water vapor was to inhibit the non-selective oxidation of C_3H_6 by O_2, and thus more C_3H_6 hydrocarbons were made available to selectively react with NO. This analysis is verified by our data which demonstrated that the $S_{SCR\text{-}HC}$ values achieved over the Cu(4)/Ag(1)/CeO_2(75)-ZrO_2(25) catalyst at 400 °C in the dry and wet conditions were 18.9% and 22.6% (data not shown), respectively. Higher $S_{SCR\text{-}HC}$ value obtained by the Cu(4)/Ag(1)/CeO_2(75)-ZrO_2(25) catalyst in wet condition clearly indicated that more C_3H_6 were available in this condition to selectively reduce NO and thus slightly gave rise to the NO conversion with time on stream.

4. Conclusion

Over a series of CeO_2-ZrO_2 catalysts with various Zr contents, CeO_2(75)-ZrO_2(25) catalyst was found to be a suitable support for NO reduction catalyst due to its high reducibility to activate C_3H_6 to selectively reduce NO in the presence of excess O_2. In comparison with Cu(4)/Ag(1)/CeO_2 catalyst, Cu(4)/Ag(1)/CeO_2(75)-ZrO_2(25) catalyst showed higher NO reduction activity especially in the low temperature region. The strong metal-support interaction and high reducibility of the support shown by Cu(4)/Ag(1)/CeO_2(75)-ZrO_2(25) catalyst were believed to improve its performance. The central composite design coupled with response surface methodology was utilized to predict the optimum values of process parameters for maximum NO conversion. Reaction temperature was found to affect the NO reduction activity more significantly than NO and C_3H_6 concentrations. The optimum conditions were estimated to be 415.38 °C reaction temperature, 1827.16 ppm of NO concentration and 1908.13 ppm of C_3H_6 concentration corresponding to NO conversion of 82.89%. In the presence of water vapor, the Cu(4)/Ag(1)/CeO_2(75)-ZrO_2(25) catalyst was more tolerant than the Cu(4)/Ag(1)/CeO_2 catalyst.

Acknowledgement

The authors gratefully acknowledge the financial support received in the form of a research grant (Project Number: 09-02-06-0008 EA008; Vote 74012) from the Ministry of Science, Technology and Innovation, Malaysia.

References

[1] S. Matsumoto, Catal. Today 29 (1996) 43.
[2] P. Engström, A. Amberntsson, M. Skoglundh, E. Fridell, G. Smedler, Appl. Catal. B 22 (1999) 241.
[3] J.G. Cohn, D.R. Steele, H.C. Andersen, US Patent 2,975,025 (1961).
[4] M. Shelef, Chem. Rev. 95 (1995) 209.
[5] J.N. Armor, Appl. Catal. B 1 (1992) 221.
[6] J.N. Armor, Catal. Today 26 (1995) 147.
[7] G.B.F. Seijger, P. Van Kooten Niekerk, K. Krishna, H.P.A. Calis, H. Van Bekkum, C.M. Van den Bleek, Appl. Catal. B 40 (2003) 31.
[8] C. Shi, M. Cheng, Z. Qu, X. Yang, X. Bao, Appl. Catal. B 36 (2002) 173.
[9] P. Carniti, A. Gervasini, V.H. Modica, N. Ravasio, Appl. Catal. B 28 (2000) 175.
[10] G. Ferraris, G. Fierro, M.L. Jacono, M. Inversi, R. Gragone, Appl. Catal. B 45 (2003) 91.
[11] M. Iwamoto, H. Hamada, Catal. Today 10 (1991) 57.
[12] J. Kašpar, P. Fornasiero, M. Graziani, Catal. Today 50 (1999) 285.
[13] N. Hickey, P. Fornasiero, J. Kašpar, M. Graziani, G. Martra, S. Coluccia, S. Biella, L. Prati, M. Rossi, J. Catal. 209 (2002) 271.
[14] R. Di Monte, P. Fornasiero, J. Kašpar, P. Rumori, G. Gubitosa, M. Graziani, Appl. Catal. B 24 (2000) 157.
[15] G. Ranga Rao, P. Fornasiero, R. Di Monte, J. Kašpar, G. Vlaic, G. Balducci, S. Meriani, G. Gubitosa, A. Cremona, M. Graziani, J. Catal. 162 (1996) 1.
[16] R. Di Monte, P. Fornasiero, J. Kašpar, M. Graziani, J. Alloys Compd. 275–277 (1998) 877.

[17] A.B. Hungria, A. Iglesias-Juez, A. Martínez-Arias, Fernández-García, J.A. Anderson, J.C. Conesa, J. Soria, J. Catal. 206 (2002) 281.
[18] G.P. Ansell, A.F. Diwell, S.E. Golunski, J.W. Hayes, R.R. Rajaram, T.J. Truex, A.P. Walker, Appl. Catal. B 2 (1993) 81.
[19] J.A. Sullivan, J. Cunningham, Appl. Catal. B 15 (1998) 275.
[20] J.Y. Yan, W.M.H. Sachtler, H.H. Kung, Catal. Today 33 (1997) 279.
[21] Z. Chajar, P. Denton, F.B. de Bernard, M. Primet, H. Praliaud, Catal. Lett. 55 (1998) 217.
[22] N.A. Saidina Amin, E.F. Tan, Z.A. Manan, Appl. Catal. B 43 (2003) 57.
[23] N.A. Saidina Amin, E.F. Tan, Z.A. Manan, J. Catal. 222 (2004) 100.
[24] I.H. Son, M.C. Kim, H.L. Koh, K.-L. Kim, Catal. Lett. 75 (2001) 191.
[25] C. de Leitenburg, A. Trovarelli, J. Llorca, F. Cavani, G. Bini, Appl. Catal. A 139 (1996) 161.
[26] D. Terribile, A. Trovarelli, C. de Leitenburg, A. Primavera, G. Dolcetti, Catal. Today 47 (1999) 133.
[27] S.S. Deshmukh, M. Zhang, V.I. Kovalchuk, J.L. d'Itri, Appl. Catal. B 45 (2003) 135.
[28] X. Tang, B. Zhang, Y. Li, Y. Xu, Q. Xin, W. Shen, Catal. Today 93–95 (2004) 191.
[29] K. Otsuka, W. Ye, M. Nakamura, Appl. Catal. A 183 (1999) 317.
[30] S. Rossignol, Y. Madier, D. Duprez, Catal. Today 50 (1999) 261.
[31] P. Fornasiero, G. Balducci, R. Di Monte, J. Kašpar, V. Sergo, G. Gubitosa, A. Ferrero, M. Graziani, J. Catal. 164 (1996) 173.
[32] M. Thammachart, V. Meeyoo, T. Risksomboon, S. Osuwan, Catal. Today 68 (2001) 53.
[33] F. Boccuzzi, A. Chiorino, G. Martra, M. Gargano, N. Ravasio, B. Carrozzini, J. Catal. 165 (1997) 129.
[34] M. Shimokawabe, H. Asakawa, N. Takezawa, Appl. Catal. 59 (1990) 45.
[35] L. Chen, T. Horiuchi, T. Osaki, T. Mori, Appl. Catal. B 23 (1999) 123.
[36] J.A. Anderson, C. Márquez-Alvarez, M.J. López-Muñoz, I. Rodríguez-Ramos, A. Guerrero-Ruiz, Appl. Catal. B 14 (1997) 189.
[37] A. Jones, B. McNicol, Temperature Programmed Reduction for Solid Materials Characterization, Dekker, New York, 1986, p. 81.
[38] C.-C. Chien, W.-P. Chuang, T.-J. Huang, Appl. Catal. A 131 (1995) 73.
[39] C.E. Hori, H. Permana, K.Y. Simon Ng, A. Brenner, K. More, K.M. Rahmoeller, D. Belton, Appl. Catal. A 16 (1998) 105.
[40] J. Kaspar, P. Fornasiero, N. Hickey, Catal Today 77 (2003) 419.
[41] K. Shimizu, J. Shibata, H. Yoshida, A. Satsuma, T. Hattori, Appl. Catal. B 30 (2001) 151.
[42] E. Bekyarova, P. Fornasiero, J. Kašpar, M. Graziani, Catal. Today 45 (1998) 179.
[43] D.D. Khoo, A.R. Mohamed, S. Bhatia, Chem. Eng. J. 103 (2004) 147.
[44] S.R. Brown, L.E. Melemed, Experimental Design and Analysis, Quantitative Application in the Social Sciences, vol. 74, Sage Publication, California, 1990, p. 12.
[45] R. Burch, J.P. Breen, F.C. Meunier, Appl. Catal. B 39 (2002) 283.
[46] K. Shimizu, A. Satsuma, T. Hattori, Appl. Catal. B 25 (2000) 239.
[47] M.C. Kung, P.W. Park, D.W. Kim, H.H. Kung, J. Catal. 181 (1999) 1.
[48] M. Haneda, Y. Kintaichi, H. Hamada, Catal. Lett. 55 (1998) 47.